IEEE Access
Multidisciplinary | Rapid Review | Open Access Journal

Received February 1, 2019, accepted February 20, 2019, date of publication February 26, 2019, date of current version March 25, 2019.

Digital Object Identifier 10.1109/ACCESS.2019.2901721

A High-Gain Sparse Phased Array With Wide-Angle Scanning Performance and Low Sidelobe Levels

YOU-FENG CHENG[1], XIAO DING[2], (Member, IEEE), WEI SHAO[2], (Member, IEEE), AND CHENG LIAO[1], (Member, IEEE)

[1]Institute of Electromagnetics, Southwest Jiaotong University, Chengdu 610031, China
[2]School of Physics, University of Electronic Science and Technology of China, Chengdu 610054, China

Corresponding author: You-Feng Cheng (juvencheng@swjtu.edu.cn)

This work was supported in part by the National Natural Science Foundation of China under Grant 61731005 and Grant 61771407, and in part by the Aeronautical Science Foundation of China under Grant ASFC-20162080008.

ABSTRACT This paper introduces the concept of the sparse array into the design of a wide-angle scanning phased array to obtain the low sidelobe level (SLL). The adopted array element is a half-mode substrate integrated waveguide slot array, which can radiate a high-gain and wide-beam pattern in the E-plane. A 16-element phased array with an optimized non-periodic array element arrangement, which is obtained by a semi-full-wave simulation-based synthesis method, is designed and studied. Compared with two periodic arrays with the same array element and element number, the sparse one exhibits the advantage of low SLL. Besides, the designed phased array has an ultra-low profile of only about $0.017\lambda_0$. A prototype is fabricated and measured, and measured results show that the proposed array can scan its main beam from $-70°$ to $+70°$ with a realized gain higher than 18.2 dBi and peak SLL lower than -15 dB.

INDEX TERMS Half-mode substrate integrated wavguide (HMSIW), low sidelobe level (SLL), sparse array, wide-angle scanning phased array.

I. INTRODUCTION

Phased arrays have been studied for several decades due to their adaptive beamforming by adjusting the input phase. In summary, phased arrays have some unique features of fast wide-angle scanning without moving the antenna, graceful degradation in performance over time, distributed aperture, multiple beams and potential for low radar cross section [1]. As one of the branches, planar phased arrays have got great interest because of their attractive characteristics such as planar structure, low cost, low profile, and ease of fabrication. However, broadening the beam scanning range of a planar phased array is a strong challenge [2].

In previous researches, many solutions have been suggested. For instance, planar arrays based on the image theory [3]–[5] and surface-wave assisted arrays based on the high-impedance surface (HIS) [6], are investigated as efficient wide-scan methods. These designs are capable of broadening the element radiation beamwidth. Recently, pattern reconfigurable elements, which can change the antenna radiation pattern by adjusting the current distribution with other antenna characteristics unchanged, are introduced into the design of wide-angle scanning arrays [7]–[9]. However, there is a common problem in these methods, namely the trade-off between the sidelobe level (SLL) and the realized gain. In [3]–[6], in order to avoid unnecessary grating lobes, the inter-element distance is selected much less than the half free-space wavelength, which results in low array gain due to the small radiation aperture. The inter-element spacing of the designs in [7]–[9] can be chosen larger than the half free-space wavelength and high array gain can be obtained. Nevertheless, high sidelobe would generally emerge in these cases. Thus amplitude tapering is often utilized to reduce the SLLs, which results in poor total efficiency.

These above solutions are mainly realized with special elements, such as the wide-beam and joint wide-beam antennas. Based on the traditional principle of pattern multiplication, the array factor is also an important part to determine the array performance besides the element factor. It is well known that aperiodic arrays have the potential ability to realize

The associate editor coordinating the review of this manuscript and approving it for publication was Lu Guo.

low SLL [10]–[18]. Therefore, it is feasible to introduce the concept of the aperiodic array into designs of wide-angle scanning phased arrays. In [19], a weighted and thinned linear array based on pattern reconfigurable elements, which can scan its main beam from −60° to +60° in the elevation plane, was presented. The SLL is efficiently reduced but still higher than −10 dB in the high-elevation area. Reference [20] adopted the concept of random subarrays and designed a dual-band wide-angle scanning phased array. The designed array has a SLL lower than −10 dB for all the scanning angles. However, the amplitude-phase synthesis is used.

In this work, a high-gain and low-profile phased array with wide-angle scanning and low SLL is presented. Firstly, a half-mode substrate integrated waveguide (HMSIW) slot array antenna with wide beam and high gain is designed as the array element. Secondly, a semi-full-wave simulation-based synthesis method is presented. Based on the minimum inter-element distance which is determined to obtain low mutual coupling (MC) between adjacent elements, the element locations are then optimized to realize the SLL reduction. Finally, the designed phased array is presented, and it is compared with two periodic arrays with the same array element and element number to validate the sidelobe reduction function of the sparse array structure. The proposed array is simulated, fabricated and measured, and the measured results validate the wide-angle scanning, low-SLL and high-gain performance.

II. HMSIW SLOT ELEMENT DESIGN AND ANALYSIS

Generally, there are three noteworthy features of the design of a wide-angle scanning phased array, namely, the broad-beam element, low mutual coupling effect and small element distance to avoid grating lobes. In this design, the first feature is realized through a HMSIW slot element whose radiation performance would be extensively studied in this section. The second one is realized with a selected minimum inter-element distance and the ultra-thin array structure, the former makes the mutual coupling between adjacent elements be lower than −20 dB and the latter leads to a low surface-wave coupling. The last restrictive condition can be eliminated with the sparse array structure which is able to realize low sidelobe by optimization.

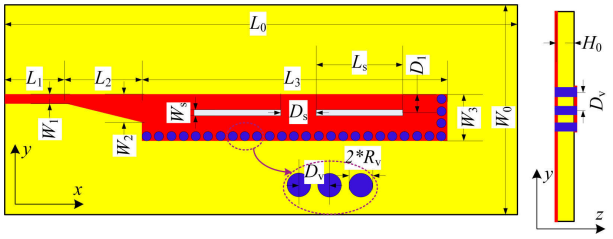

FIGURE 1. Geometry of the HMSIW slot element.

The geometry of the proposed HMSIW slot element is shown in Fig. 1. A rectangle patch with a length of L_3 and a width of W_3, several metal vias with a radius of R_v and a ground plane form the HMSIW cavity. Two rectangle slots are etched on the patch with a distance of D_s and generate the far-field radiation. The slots are fed with a rectangle and a tapering strips. The substrate has a thickness of H_0 and a relative dielectric constant of 2.65. The optimized geometry parameters are: L_0 = 150mm, L_1 = 25mm, L_2 = 15mm, L_3 = 90mm, L_s = 24mm, W_0 = 100mm, W_1 = 2.5mm, W_2 = 9.8mm, W_3 = 13.25mm, W_s = 1.5mm, D_1 = 3.25mm, D_s = 16mm, D_v = 1.5mm, R_v = 0.5mm, and H_0 = 1mm.

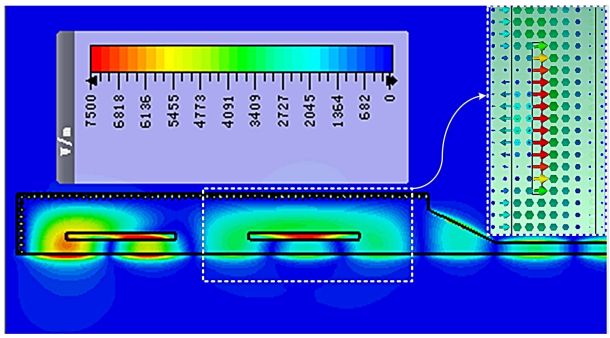

FIGURE 2. Simulated E-field distribution on the patch.

Fig. 2 illustrates the simulated E-field distribution on the rectangle patch. It can be seen that a fundamental quasi-$TE_{0.5,0}$ mode is excited in the HMSIW [21]–[23]. Note that, compared to the full-mode SIW, the HMSIW has a half size in the x direction. This means in the array environment, the HMSIW slot element has a compact size and low mutual coupling with a certain inter-element distance.

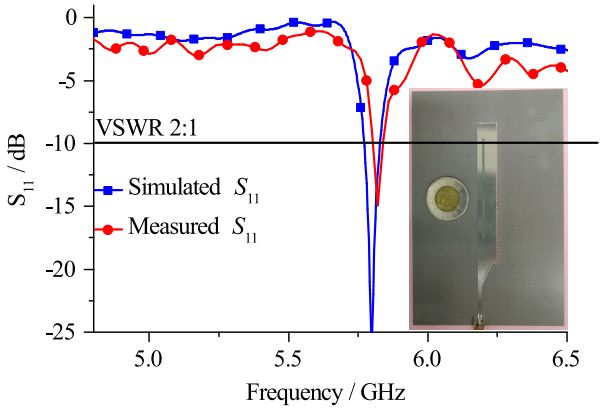

FIGURE 3. Simulated and measured S-parameters of the HMSIW slot element.

The simulated and measured reflection coefficients of the HMSIW slot element are shown in Fig. 3. The measured results agree well with the simulated ones. It can be seen that the HMSIW slot element can work at 5.8 GHz with a good impedance match.

The slots are etched to generate equivalent magnetic currents. It can also be observed from Fig. 2 that the electric filed in the radiation slots goes from one long side to the other side. According to the principle of equivalence, for each

slot, the electric field in the slot can be equivalent to magnetic current

$$\vec{M}_x = -\vec{n}_z \times \vec{E}_y \tag{1}$$

where n_z is the unit vector in the z direction, and E_y is the electric field in the slot. Furthermore, with respect to the E-field distribution shown in Fig. 2, the equivalent magnetic current in the slot can be assumed to be

$$\vec{M}_x = \vec{n}_x M_0 \delta(y, z) \tag{2}$$

where n_x is the unit vector in the x direction, M_0 is the magnetic current amplitude, and $\delta(y, z)$ is the three-dimensional delta function. Then, the electric vector potential generated by the magnetic current source can be calculated by

$$\vec{F} = \frac{1}{4\pi} \int_v \frac{\vec{M}_x}{r} e^{-jkr} dv \tag{3}$$

and thus the far-field electric field can be given as

$$\vec{E}_m = -\nabla \times \vec{F} \tag{4}$$

Therefore, the far-fields radiated from one slot can be calculated by

$$\begin{cases} E_\theta = \dfrac{jke^{(-jkr)} \sin\phi}{4\pi r} \displaystyle\int_{-L_s/2}^{L_s/2} M_0 \delta(y, z) e^{jkx \sin\theta \cos\phi} dx \\ E_\phi = \dfrac{jke^{(-jkr)} \cos\theta \cos\phi}{4\pi r} \displaystyle\int_{-L_s/2}^{L_s/2} M_0 \delta(y, z) e^{jkx \sin\theta \cos\phi} dx \end{cases} \tag{5}$$

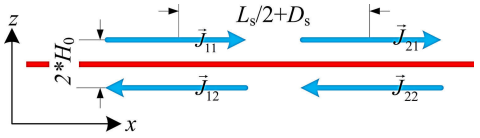

FIGURE 4. Distribution of the equivalent magnetic currents in the slots and their imaginary currents.

Finally, if the electric field in each slot is assumed to be transverse with a distribution which is equiphase and cosinusoidal in amplitude and the internal higher order mode coupling between adjacent slots is ignored, the total far fields of the proposed HMSIW slot element is a superposition of the radiations of four magnetic currents as shown in Fig. 4 [24]. Note that the upper magnetic currents are the equivalent two in the slots as shown in Fig. 1(a), and the lower two are their imaginary currents.

Fig. 5 depicts the calculated, simulated and measured normalized radiation patterns of the HMSIW slot element. In the yoz plane, the calculated results indicate that the element has a wide beam, and the simulated and measured results validate that the 3-dB beamwidth is wider than 130°. Note that the difference between the calculated, simulated and measured results may mainly because of the infinite ground size and the edge effects. The measured realized gain of the element is 9.5 dBi, which makes the element have the potential for the design of a high-gain phased array.

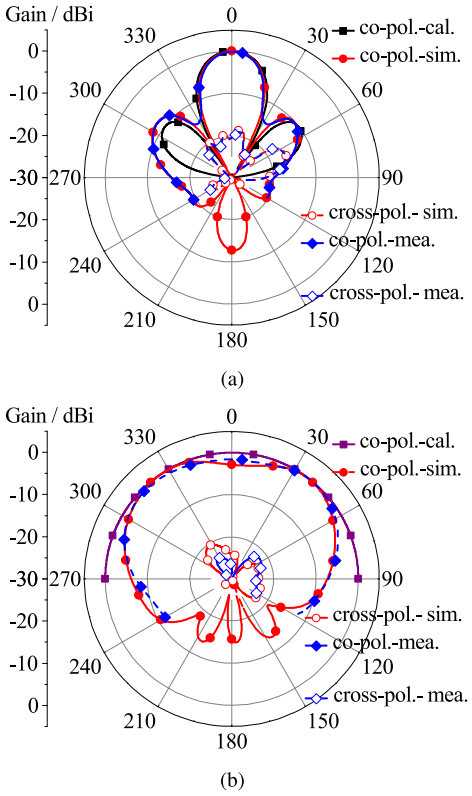

FIGURE 5. Calculated, simulated and measured normalized radiation patterns of the HMSIW slot element. (a) *xoz* plane. (b) *yoz* plane.

III. SPARSE PHASED ARRAY DESIGN

The main purpose of using the sparse array structure is to reduce the sidelobes of the scanning beams. It is reported in [16]–[18] that the sidelobes should be bounded by the peak SLL at the furthest scan angle when the array beam is steered between broadside and the maximum scan angle. This conclusion is proved for the first time by using the Poisson sum formula in this paper. For simplicity, only the array factor in the absence of the MC effects is considered. Assuming an sparse linear array with N elements, the radiation pattern can be given by

$$F(\theta) = \sum_{n=1}^{N} A_n e^{j(kd_n \sin\theta - \varphi)} \tag{6}$$

where A_n and φ_n are, respectively, the current amplitude and phase in the nth element, d_n is the element position of the nth element. By using Fourier transform, (6) can be converted as [25], [26]

$$\begin{cases} F(\theta) = \displaystyle\sum_{\substack{m=-\infty \\ \varepsilon+N}}^{+\infty} E_m(k \sin\theta) \\ E_m(\theta) = \displaystyle\int_{\varepsilon} A_v e^{j(kd_v \sin\theta - \varphi_v)} e^{j2m\pi v} dv \end{cases} \tag{7}$$

here $E_0(u)$ represents the main beam and $E_i(u)$, $i \neq 0$ represents the grating lobes. Thus the greatest grating lobe is

$$GF(\theta) = \max\left(\int_{\varepsilon}^{\varepsilon+N} A_v e^{j[kd_v \sin\theta - (\varphi_0 + \Delta\varphi_v)]} e^{j2m\pi v} dv \right) \quad (8)$$

It can be found from (8) that $GF(\theta)$ increases with the increase of the phase difference $\Delta\varphi_v$) between the vth element and the first element, which means a larger phase difference would result in a higher SLL. In other words, the generated SLL increases when a phased array scans from the broadside direction to the high-elevation angle. This conclusion is consistent with that reported in [11]–[13].

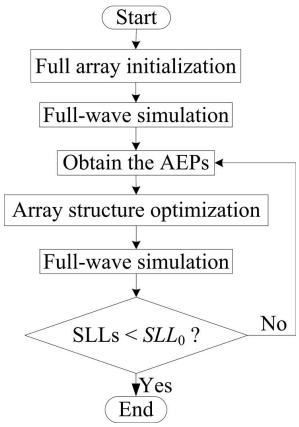

FIGURE 6. Flowchart of the semi-full-wave simulation-based synthesis method.

In the array synthesis, the main-beam direction can be fixed as a value which is a little higher than the maximum scan angle (here chosen as 75°). The proposed synthesis method shown in Fig. 6 starts from an initial periodic array with a inter-element distance of $\Delta d = 0.75\lambda_0$. Full-wave simulation is used to obtain the active element patterns (AEPs) but only performed for the array layout before the optimization. In the optimization, element position perturbations are used to realize a new array structure and Δd always retains between $0.45\lambda_0$ and $1.5\lambda_0$. The purpose of that the minimum inter-element distance is selected as $0.45\lambda_0$ is to generate low MC between the elements. Besides, the above simulated AEPs are still implemented for the array elements in the optimization. Particle swarm optimization (PSO) algorithm is adopted for the array structure optimization. Next, the newly generated array layout is simulated and the SLLs can be obtained. If the simulated SLLs in the pattern mask are all lower than a target value SLL_0 (here selected as -15 dB), then the final array configuration is realized. Otherwise, the AEPs of current array layout are updated from the simulation as decried above, and the iteration continues to reach convergence. The full-wave simulation is not always performed in the optimization, which greatly reduces the computation burden and time. In addition, the MC effects are included in the synthesis.

TABLE 1. Optimized array element locations.

Element	Location	Element	Location	Element	Location
2	$1.5\lambda_0$	3	$1.95\lambda_0$	4	$2.4\lambda_0$
5	$2.85\lambda_0$	6	$3.3\lambda_0$	7	$3.75\lambda_0$
8	$4.2\lambda_0$	9	$4.65\lambda_0$	10	$5.1\lambda_0$
11	$5.55\lambda_0$	12	$6.017\lambda_0$	13	$6.467\lambda_0$
14	$6.917\lambda_0$	15	$7.367\lambda_0$	16	$7.873\lambda_0$

In the PSO, the acceleration coefficients $c1$ and $c2$ are both chosen as 2. After the synthesis, a 16-element sparse linear array is generated. The element locations of the optimized array layout is shown in Table 1, and an array prototype is fabricated as shown in Fig. 7. It can be found that most of the inter distances are the minimum inter spacing ($0.45\lambda_0$), and a few elements are optimized with a large inter distances (the largest one is $1.5\lambda_0$) away from their adjacent elements.

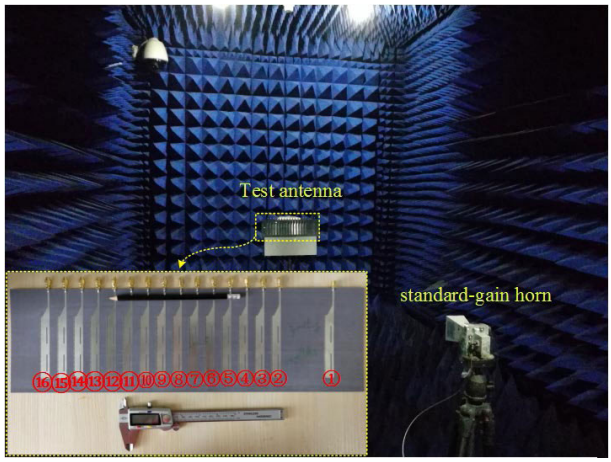

FIGURE 7. Fabricated Prototype and its measurement environment.

It should be noted that any element antennas, which satisfy three noteworthy features of the design of a wide-angle scanning phased array (the broad-beam element, low mutual coupling effect and small element distance to avoid grating lobes), can be chosen for the array element. The sparse design method can be applied to any wide-angle scanning phased arrays.

IV. EXPERIMENTAL SPARSE ARRAY PERFORMANCE

A. REFLECTION AND ISOLATION PERFORMANCE

Firstly, the array element reflection performance and the array active reflection performance are measured and studied to illustrate that the MC between the array elements are quite low and no scan blindness appears in a wide-scan range. These S-parameters are measured using an AV3618 Vector Network Analyzer.

Due to the non-periodic array structure, Fig. 8 shows the measured isolated reflection coefficients of all the array elements and the isolation between all the adjacent elements. From the measured results, all the elements is able to operate at 5.8 GHz with low reflection. In addition, the MC between

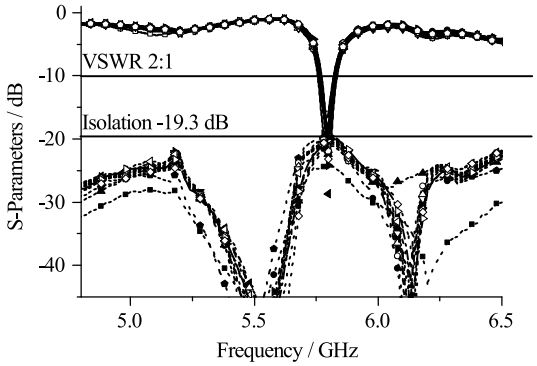

FIGURE 8. Measured S-parameters of all the array elements.

arbitrary two elements can be deduced to be lower than −19.3 dB. It is worth noting that the low profile benefits for the low MC, because the surface-wave coupling is generally strong in a thick substrate.

Another important factor which can explain the no-scan blindness property of the phased array is the active reflection coefficient. when the phased array scans to θ_0, the active reflection coefficient of the mth element can be written as [21]

$$\Gamma_m = e^{(jk_0 m x_m \sin\theta_0)} \sum_{n=1}^{16} S_{mn} e^{(-jk_0 n x_n \sin\theta_0)} \tag{9}$$

where S_{mn} is the (m, n)th element of the scattering matrix, x_m and x_n are the positions of the mth and nth element, k_0 is the free-space wavenumber, and θ_0 is the current scanning angle. Fig. 9 plots the calculated active reflection coefficients of elements 4, 8, 9 and 12. At 5.8 GHz, the reflection always retain lower than −10 dB when the phased array scans in a range from −70° to +70°. It can be construed that the beam scanning up to a maximum angle of ±70° can be still realistically expected from the designed array and no scan blindness appears.

B. BEAM SCANNING PERFORMANCE

Secondly, the array scanning patterns are measured and the wide-scan ability is studied. AEPs of all the elements are measured in an anechoic chamber to calculate the far-filed scanning patterns. As shown in Fig. 7, a standard-gain horn is used as the receiver and the phased array is the transmitter. The radiation pattern of the whole array can be calculated as a superposition of the AEPs of all elements, which is given as

$$E_{array} = \sum_{n=1}^{16} W_n E_n(\theta, \varphi) e^{j(k\hat{r}\cdot r_n - \phi_n)} \tag{10}$$

where E_n is the AEP of the nth element, W_n and ϕ_n represent the input amplitude and phase, respectively.

The measured AEPs of Elements 4, 8, 9 and 12 are shown in Fig. 11. It can be seen that all the AEPs exhibit wide-beam and high-gain performance, which are suitable for designs of high-gain and wide-angle scanning phased arrays. Compared

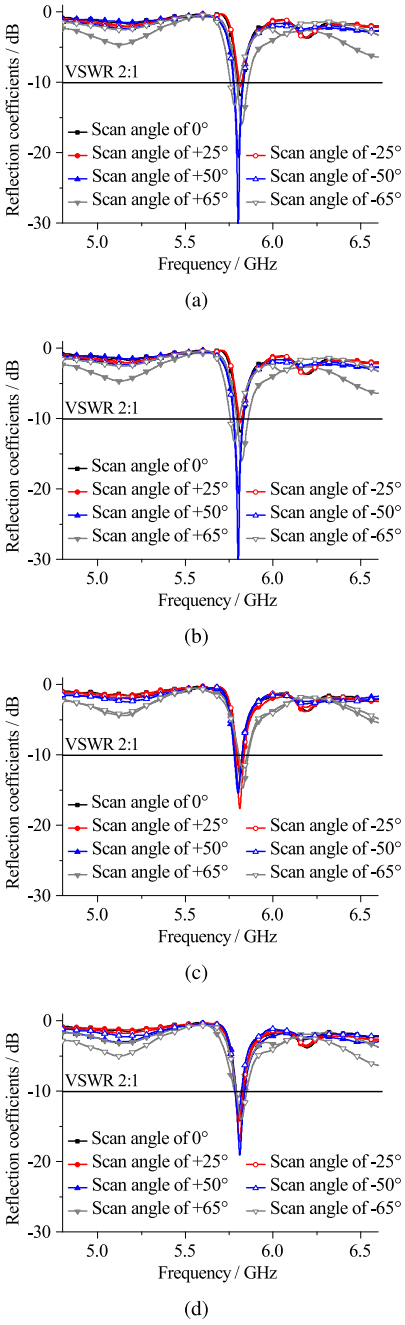

FIGURE 9. Calculated active reflection coefficients of partial array elements. (a) Element 4. (b) Element 8. (c) Element 9. (d) Element 12.

with the single element patterns shown in Figure 5, the measured AEPs also have wide radiation beams and high gains. Besides, the cross-polarization components of the measured AEPs are a little higher (less than 1.5 dB) than those of single element patterns.

The measurement-based calculated results with uniform input amplitudes and linear input phases are depicted in Fig. 10, from which the calculated ones agree well with the simulated ones. It can be concluded that the phased array supports a main beam coverage from −70° to +70°.

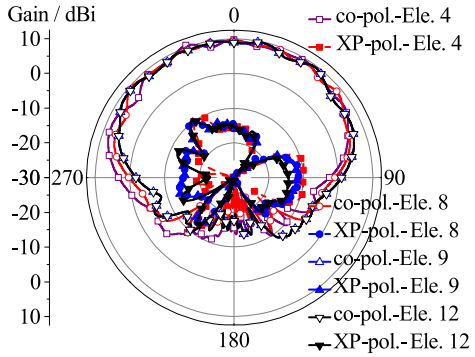

FIGURE 10. Measured active element patterns of elements 4, 8, 9, and 12.

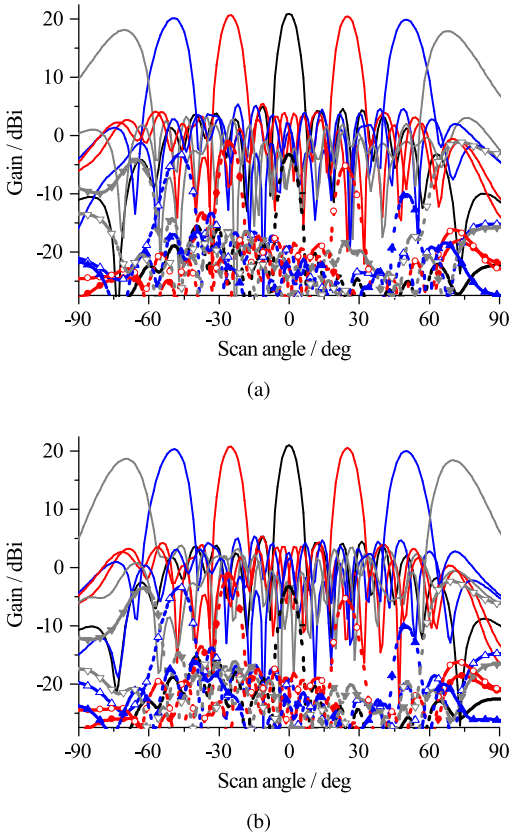

FIGURE 11. Simulated and calculated scanning beams of the designed phased array. (a) Simulated results. (b) Calculated results. (Here solid lines represent the co-polarized patterns and dotted lines represent the cross-polarized patterns).

When the scan angle increases, the realized array gain drops from 21 to 18.2 dBi. In the array scanning range, the peak SLL is always lower than −15 dB. Detailed array scanning characteristics including the realized gain, peak SLL and half-power beamwidth (HPBW) are listed in Table 2.

Scanning characteristics comparisons between the designed sparse array and two periodic phased arrays are listed in Table 3. Note that the Periodic arrays 1 and 2 represent periodic linear arrays with inter-element distances of $0.45\lambda_0$ and $0.75\lambda_0$, respectively. Compared with Periodic array 1, the designed array has a 5-dB-lower peak SLL, and its peak gain and scanning range have a little advantage. In terms of the scanning performance of the designed array and Periodic array 2, the former one has great advantages in the scanning range and peak SLL at the expense of the peak gain. In summary, the sparse array layout is advantageous to realize the low-SLL performance in the wide-angle scanning range.

TABLE 2. Scanning characteristics of the phased array with uniform input amplitudes and linear input phases.

Scan angle (deg)	Peak gain (dBi)	Peak SLL (dB)	HPBW (deg)
0	21.0	-15.7	6.6
-25	20.8	-15.5	7.2
-50	20.3	-15.2	10.3
-70	18.5	-15.1	14.6
+25	20.6	-16.3	7.6
+50	20.1	-15.4	10.2
+70	18.2	-15.1	14.4

TABLE 3. Scanning characteristics comparison between the designed phased array and periodic arrays with the same element and element number.

Phased arrays	Scan range (deg)	Peak gain (dBi)	Peak SLL (dB)
Designed	-70 ∼ + 70	21.0	-15.1
Periodic array 1	-69 ∼+ 69	20.8	-10.2
Periodic array 2	-55 ∼ +55	21.5	-4.8

TABLE 4. Comparison of wide-angle scanning performance between this paper and [19], [20], and [27].

Reference	Peak gain/element number	Peak SLL	Scan range
[19]	13.2 dBi / 8	-5.3	-60° ∼ +60°
[20]	15.8 dBi / 16	-10.2	-75° ∼ +75°
[27]	10.2 dBi / 8	-7.7	-78° ∼ +78°
This paper	21.0 dBi / 16	-15.1	-70° ∼ +70°

Also, a detailed comparison between the proposed phased array and those in [19], [20], and [27] are shown in Table 4. Designs in [19] and [27] are based on pattern reconfigurable elements (PREs) and those in [20] and this paper adopt the wide-beam elements (WBEs). Besides, phased arrays in [19] and [20], and this paper have aperiodic array layouts, and that in [27] is a periodic design. It can be seen that the proposed design possesses a wider scanning range than that in [19] and its scanning range is a little narrower than those in [20] and [27]. However, the proposed design has the highest realized gain and lowest PSL.

At last, it should be noted that, an HMSIW slot antenna does have the potential to exhibit the band-enhanced and dual-band performance [27], [28]. However, the proposed wide-angle scanning phased array based on the narrow-band HMSIW slot antenna can also be used as receivers in some practical applications.

V. CONCLUSION

In this communication, a sparse linear phased array with wide-angle scanning, high-gain, low-profile and low-SLL performance is designed and studied. Firstly, a HMSIW slot

array element is designed. The antenna radiation property is investigated to show the wide HPBW. Then, the sparse array optimization procession including a semi-full-wave simulation-based synthesis method is presented. Besides, before the synthesis, a Poisson sum formula-based proof is proposed to reveal that the sidelobes should be bounded by the peak SLL at the furthest scan angle when the array beam is steered between broadside and the maximum scan angle. Next, the sparse wide-angle scanning phased array based on the HMSIW element is presented. The measured results indicate that the phased array supports a main beam coverage from $-70°$ to $+70°$ with the SLL lower than -15 dB all the time. At last, some comparisons between the designed array and two periodic arrays are given. It can be concluded that the sparse array layout is advantageous to realize the low-SLL performance in the wide-angle scanning range.

REFERENCES

[1] R. L. Haupt and Y. Rahmat-Samii, "Antenna array developments: A perspective on the past, present and future," *IEEE Antennas Propag. Mag.*, vol. 57, no. 1, pp. 86–96, Feb. 2015.

[2] A. G. Toshev, "Multipanel concept for wide-angle scanning of phased array antennas," *IEEE Trans. Antennas Propag.*, vol. 56, no. 10, pp. 3330–3333, Oct. 2008.

[3] R. Wang, B.-Z. Wang, X. Ding, and X.-S. Yang, "Planar phased array with wide-angle scanning performance based on image theory," *IEEE Trans. Antennas Propag.*, vol. 63, no. 9, pp. 3908–3917, Sep. 2015.

[4] J. Liu and Q. Xue, "Microstrip magnetic dipole Yagi array antenna with endfire radiation and vertical polarization," *IEEE Trans. Antennas Propag.*, vol. 61, no. 3, pp. 1140–1147, Mar. 2013.

[5] Y. Q. Wen, B. Z. Wang, and X. Ding, "A wide-angle scanning and low sidelobe level microstrip phased array based on genetic algorithm optimization," *IEEE Trans. Antennas Propag.*, vol. 64, no. 2, pp. 805–810, Feb. 2016.

[6] M. Li, S.-Q. Xiao, and B.-Z. Wang, "Investigation of using high impedance surfaces for wide-angle scanning arrays," *IEEE Trans. Antennas Propag.*, vol. 63, no. 7, pp. 2895–2901, Jul. 2015.

[7] X. Ding, B.-Z. Wang, and G.-Q. He, "Research on a millimeter-wave phased array with wide-angle scanning performance," *IEEE Trans. Antennas Propag.*, vol. 61, no. 10, pp. 5319–5324, Oct. 2013.

[8] A. Pal, A. Mehta, D. Mirshekar-Syahkal, and H. Nakano, "2 × 2 phased array consisting of square loopantennas for high gain wide angle scanning-with low grating lobes," *IEEE Trans. Antennas Propag.*, vol. 65, no. 2, pp. 576–583, Feb. 2017.

[9] Y.-F. Cheng, X. Ding, W. Shao, and B.-Z. Wang, "Planar wide-angle scanning phased array with pattern-reconfigurable windmill-shaped loop elements," *IEEE Trans. Antennas Propag.*, vol. 65, no. 2, pp. 932–936, Feb. 2017.

[10] Y. V. Krivosheev, A. V. Shishlov, and V. V. Denisenko, "Grating lobe suppression in aperiodic phased array antennas composed of periodic subarrays with large element spacing," *IEEE Trans. Antennas Propag.*, vol. 57, no. 1, pp. 76–85, Feb. 2015.

[11] B. K. Chang, X. Ma, and H. B. Sequeira, "Minimax-maxmini algorithm: A new approach to optimization of the thinned antenna arrays," in *Proc. AP-S Int. Symp. Dig.*, vol. 1, Jun. 1994, pp. 514–517.

[12] R. L. Haupt, "Thinned arrays using genetic algorithms," *IEEE Trans. Antennas Propag.*, vol. 42, no. 7, pp. 993–999, Jul. 1994.

[13] M. G. Bray, D. H. Werner, D. W. Boeringer, and D. W. Machuga, "Optimization of thinned aperiodic linear phased arrays using genetic algorithms to reduce grating lobes during scanning," *IEEE Trans. Antennas Propag.*, vol. 50, no. 12, pp. 1732–1742, Dec. 2002.

[14] S. Caorsi, A. Lommi, A. Massa, and M. Pastorino, "Peak sidelobe level reduction with a hybrid approach based on GAs and difference sets," *IEEE Trans. Antennas Propag.*, vol. 52, no. 4, pp. 1116–1121, Apr. 2004.

[15] K. C. Kerby and J. T. Bernhard, "Sidelobe level and wideband behavior of arrays of random subarrays," *IEEE Trans. Antennas Propag.*, vol. 54, no. 8, pp. 2253–2262, Aug. 2006.

[16] R. L. Haupt, "Optimized weighting of uniform subarrays of unequal sizes," *IEEE Trans. Antennas Propag.*, vol. 55, no. 4, pp. 1207–1210, Apr. 2007.

[17] N. Jin and Y. Rahmat-Samii, "Advances in particle swarm optimization for antenna designs: Real-number, binary, single-objective and multiobjective implementations," *IEEE Trans. Antennas Propag.*, vol. 55, no. 3, pp. 556–567, Mar. 2007.

[18] A. B. Smolders and H. J. Visser, "Low side-lobe circularly-polarized phased arrays using a random sequential rotation technique," *IEEE Trans. Antennas Propag.*, vol. 62, no. 12, pp. 6476–6481, Dec. 2014.

[19] Y. Y. Bai, S. Xiao, M. C. Tang, Z. F. Ding, and B. Z. Wang, "Wide-angle scanning phased array with pattern reconfigurable elements," *IEEE Trans. Antennas Propag.*, vol. 59, no. 11, pp. 4071–4076, Nov. 2011.

[20] Y.-F. Cheng, X. Ding, W. Shao, and B.-Z. Wang, "Dual-band wide-angle scanning phased array composed of SIW-cavity backed elements," *IEEE Trans. Antennas Propag.*, vol. 66, no. 5, pp. 2678–2683, May 2018.

[21] W. Hong *et al.*, "Half mode substrate integrated waveguide: A new guided wave structure for microwave and millimeter wave application," in *Proc. Joint 31st Int. Conf. Infr. Millim. Waves 14th Int. Conf. Teraherz Electron.*, Sep. 2006, p. 219.

[22] Q Lai, W Hong, Z. Qi Kuai, Y. S. Zhang, and K. Wu, "Half-mode substrate integrated waveguide transverse slot array antennas," *IEEE Trans. Antennas Propag.*, vol. 57, no. 4, pp. 1064–1072, Apr. 2009.

[23] K. Dhwaj, J. M. Kovitz, H. Tian, L. J. Jiang, and T. Itoh, "Half-mode cavity-based planar filtering antenna with controllable transmission zeroes," *IEEE Antennas Wireless Propag. Lett.*, vol. 17, no. 5, pp. 833–836, May 2018.

[24] R. Elliott and W. O'Loughlin, "The design of slot arrays including internal mutual coupling," *IEEE Trans. Antennas Propag.*, vol. AP-34, no. 9, pp. 1149–1154, Sep. 1986.

[25] A. Ishimaru, "Theory of unequally-spaced arrays," *IRE Trans. Antennas Propag.*, vol. AP-10, no. 6, pp. 691–702, Nov. 1962.

[26] A. Ishimaru, "Unequally spaced arrays based on the poisson sum formula," *IEEE Trans. Antennas Propag.*, vol. 62, no. 4, pp. 1549–1554, Apr. 2014.

[27] Y.-F. Cheng, X. Ding, W. Shao, M.-X. Yu, and B.-Z. Wang, "A novel wide-angle scanning phased array based on dual-mode pattern-reconfigurable elements," *IEEE Antennas Wireless Propag. Lett.*, vol. 16, pp. 396–399, Mar. 2017.

[28] G. Q. Luo, Z. F. Hu, W. J. Li, X. H. Zhang, L. L. Sun, and J. F. Zheng, "Bandwidth-enhanced low-profile cavity-backed slot antenna by using hybrid SIW cavity modes," *IEEE Trans. Antennas Propag.*, vol. 60, no. 4, pp. 1698–1704, Apr. 2012.

[29] S. Agneessens and H. Rogier, "Compact half diamond dual-band textile HMSIW on-body antenna," *IEEE Trans. Antennas Propag.*, vol. 62, no. 5, pp. 2374–2381, May 2014.

YOU-FENG CHENG was born in Anhui, China, in 1989. He received the Ph.D. degree in radio physics from the University of Electronic Science and Technology of China, Chengdu, China, in 2018. In 2017, he was a Visiting Scholar with the Mechanical Engineering Department, University of Houston, Houston, TX, USA. He joined Southwest Jiaotong University, Chengdu, in 2018. His research interests include phased arrays, reconfigurable antennas, and evolutionary algorithms.

XIAO DING received the B.S. and M.S. degrees in electronic engineering from the Guilin University of Electronic Science and Technology, Guilin, China, and the Ph.D. degree in radio physics from the University of Electronic Science and Technology of China (UESTC), Chengdu, China, in 2014. He joined UESTC, in 2014, where he is currently an Associate Professor. In 2013, he was a Visiting Scholar with the South Dakota School of Mines and Technology, SD, USA. From 2016 to 2017, he was a Visiting Scholar with the University of Houston, Houston, TX, USA. His research interests include reconfigurable antennas and its applications and phased arrays.

WEI SHAO received the M.Sc. and Ph.D. degrees in radio physics from UESTC, Chengdu, China, in 2004 and 2006, respectively, where he is currently a Professor. He was a Visiting Scholar with the Electromagnetic Communication Laboratory, Pennsylvania State University, in 2010. His research interests include computational electromagnetics and antenna design.

CHENG LIAO was born in Chongqing, China, in 1964. He received the Ph.D. degree in electromagnetic fields and microwave techniques from the University of Electronic Science and Technology of China, Chengdu, China, in 1995. From 1997 to 1998, he was a Visiting Scholar with the City University of Hong Kong, Hong Kong. He was a Professor with Southwest Jiaotong University, Chengdu, in 1998. His research interests include computational electromagnetic, electromagnetic compatibility, and antenna theory and design.